Full length article

A unifying view of bifurcations in a semiconductor laser subject to optical injection

Sebastian Wieczorek [a,*], Bernd Krauskopf [b], Daan Lenstra [a]

[a] *Faculty of Sciences, Vrije Universiteit, De Boelelaan 1081, 1081 HV Amsterdam, The Netherlands*
[b] *Department of Engineering Mathematics, University of Bristol, Bristol BS8 1TR, UK*

Abstract

We are concerned with the dynamics and bifurcations of a single-mode semiconductor laser with optical injection, modeled by three-dimensional rate equations. Key bifurcations, namely saddle-node, Hopf, period-doubling, saddle-node of limit cycle and torus bifurcations, are followed over a wide range of injection strengths and detunings for different fixed values of the linewidth enhancement factor α. In this way we present, to our best knowledge, the most far-reaching overview yet of the dynamics of injected semiconductor lasers. Our results compare very well with experimental studies and tie together information in the literature on different aspects of the behavior of optically injected lasers. © 1999 Elsevier Science B.V. All rights reserved.

1. Introduction

The idea of optical injection is that external light, usually of high monochromaticity, is injected into a laser in order to dictate certain properties of the laser's output light. This is sometimes referred to as master-slave relationship. In semiconductor lasers, external injection produces an enormous variety of phenomena and the purpose of this paper is to present a unified treatment of all these seemingly unrelated phenomena with emphasis on their global interrelationships. Optical injection has several important applications such as injection locking [1], frequency stabilization [2], linewidth narrowing and chirp reduction [3]. It is a very interesting technique from the more fundamental point of view. In spite of experimental difficulties, such as implied by the requirement of using a very stable master oscillator, the injected laser has developed into a key system for studies and demonstrations of complex nonlinear dynamics. The latter holds interesting promises, among others, for cryptography [4] and computing [5]. From a theoretical point of view it is the simplest laser system showing such a wealth of behavior. This makes the injected laser a generic system and a key

* Corresponding author. Tel.: + 31-20-444-7860; fax: + 31-20-444-7899; e-mail: sebek@nat.vu.nl

to understanding dynamical behavior in more difficult cases like a laser with external optical feedback [6].

Before 1990 optical injection was studied mainly in gas and solid state lasers [7–10], but later most of the interest was directed towards semiconductor lasers as they feature new effects and find very important applications today. Even though the problem of optical injection in semiconductor lasers is old (see [6] and references therein) there are many properties concerning its dynamics that are still far from being well understood, especially in terms of connecting links between the various different types of behaviors. Actually there is no analytical picture showing how the dynamics of an injected laser depends on parameters in its global scale. Existing studies usually focused on some small regions of parameter space, showing small and isolated pieces of a bifurcation diagram only [11–15], or presenting some particular routes to chaos [7,10,16–20]. The only map showing the various dynamical properties of this system for a relatively large range of parameters comes from experimentalists [21,22]. One reason for focusing on some particular aspects of dynamical behavior rather then on a global vision is that in many cases the original three-dimensional rate equations are impossible to examine analytically, forcing those investigators to deal with special approximations and simplifications of rate equations that could be dealt with.

At that time both analytical and experimental investigations were satisfactory and have revealed amazingly rich behavior like stable locking, coexistence of attractors, quasiperiodicity, instabilities, pulsations and many routes to chaos like period-doubling cascades, intermittency, break-up of tori, and homoclinic and heteroclinic tangencies [7–34] that demand further systematic investigation now. Especially many of these seemingly unrelated phenomena should find their place in a unified global picture. Therefore we look at this problem from a more global point of view with the purpose of showing the universal picture of the dynamics of optically injected (semiconductor) lasers. To this end we apply fundamental bifurcation theory that allows us to (i) systematically analyze the complex dynamics, (ii) put all these known pieces together and (iii) understand why and how they are related to each other.

We deal with the original *three-dimensional* rate equations and investigate how the laser dynamics depends on parameters. This is made possible by following bifurcations with the package AUTO [35], a powerful tool that allows us to map out the overall bifurcation structure in unprecedented detail. For example, we are able to compute curves of bifurcations in parameter space even if the bifurcating object is unstable. This should be contrasted with the method of producing bifurcation diagrams by simulation used in earlier works, which is time consuming and capable of catching only parts of the relevant bifurcations.

We study the dependence of the dynamics on the injected field strength K and its detuning ω from the unperturbed laser resonant frequency and the linewidth enhancement factor α which seem to have the most significant influence on the dynamics. The first two parameters can be changed during an experiment and are obvious to look at. On the other hand, there were not many attempts to study how the dynamics changes with the third parameter α [13,15]. Before we explain what the real significance of α is in this model we would like to stress that the intensity and the frequency of the steady state of the free running laser (without injection) may change only if one changes the pump current, or the temperature. However, we assume here that the pump current and temperature are held constant. Moreover we distinguish between two frequencies: (i) the free-running laser frequency ω_{sol} which then serves as the optical reference frequency with respect to which our dynamical equations will be formulated and (ii) the instantaneous resonant frequency which is a dynamical quantity influenced by the external injection. Then, under these conditions the α parameter quantifies to what extent the instantaneous resonance frequency will alter due to variations in the internal optical intensity caused by external injection. The physical principle behind this is that the refractive index depends on the inversion which in turn depends on the light intensity inside the laser. The value of the linewidth enhancement factor α is mainly a laser material property and thus cannot or only with difficulty be changed during an experiment. However, different kinds of semiconductor lasers have different α-values. For instance edge emitting diode lasers have α-values between 4 and

10, VCSELs between 2 and 3, and manufacturing semiconductor lasers with very small α approaching zero [36,37] seems to be a holy grail. Hence, following the nature of the problem, we present bifurcation curves in the (K,ω)-plane for different but fixed values of α from $\alpha = 0$ to higher values. In particular, we show how the dynamics and bifurcations become increasingly complex when α is increased. Thus we present here, to our best knowledge, a more far-reaching overview of the dynamics of injected semiconductor lasers than has ever been presented before.

An additional aim of this paper is to serve as a reference for further, more detailed studies. Therefore it gives a unified and consistent picture of the majority of bifurcations, linking various earlier results, but leaves several detailed questions for future analysis.

The paper is organized as follows. In Section 2 we discuss the rate equations we are working with. Section 3 introduces the bifurcation diagram in general terms. In Section 4 we then present bifurcation curves of stationary points, and in Section 5 those of periodic orbits. Section 6 points out routes to chaos, namely via a period-doubling cascade and the break-up of tori. We finally draw our conclusions and point to future work in Section 7.

2. Rate equations

Free-running semiconductor lasers working above threshold have two stationary points: an unstable one with zero intensity which is referred to as the OFF-point and a stable ON-point with nonzero electric field amplitude E_0, population inversion N_0 and frequency ω_{sol}. They also have an intrinsic resonance, which is characteristic for class B lasers and which is known as *relaxation oscillation* (RO) [6]. This resonance corresponds to a damped oscillatory exchange of energy between electric field and population inversion with frequency ω_R. It can easily be excited by several kinds of external perturbation such as injection or feedback, but for a free running laser it is always damped.

In this paper we study the dynamics of the three-dimensional rate equations for a single-mode class B laser with monochromatic external optical injection.

To normalize the optical field to a dimensionless quantity we express it in terms of units such that $|E_0|^2$ equals the total number of photons within the laser cavity. The electric field inside the laser is represented as

$$\mathscr{E}(\hat{t}) = \hat{E}(\hat{t})e^{i\omega_{\text{sol}}\hat{t}} + \text{c.c.}, \qquad (1)$$

where symbols with a hat are used here, for time and electric field, for reasons of later convenience. The rate equations describing the optically injected laser can be written as two equations, one for the dimensionless complex electric field envelope $\hat{E}$ and another for the population inversion N:

$$\frac{d\hat{E}}{d\hat{t}} = \tfrac{1}{2}(G - \Gamma_0)\hat{E} + \kappa E_{\text{inj}}e^{i\hat{\omega}\hat{t}}$$

$$\frac{dN}{d\hat{t}} = \frac{I}{e} - \Gamma_N N - (\text{Re}G)|\hat{E}|^2. \qquad (2)$$

Here the source term I/e accounts for the pump current, Γ_N is a carrier loss rate due to spontaneous recombination and Γ_0 is the photon loss rate from the cavity. The complex gain function G is linearized around the ON-point of the free running laser

$$G = \Gamma_0 + (1 + i\alpha)\xi(N - N_0), \qquad (3)$$

where α is the linewidth enhancement factor and $\xi = v_g \partial g / \partial N$ is the differential gain (v_g is the group velocity and g is the optical gain per unit length). The term $\kappa E_{\text{inj}}e^{i\hat{\omega}\hat{t}}$ in Eqs. (2) represents the externally injected electric field with detuning between the injected light and free running laser frequency $\hat{\omega} = \omega_{\text{inj}} - \omega_{\text{sol}}$ and the injected field rate $\kappa = t_1/\tau_{in}$, where τ_{in} is the laser cavity internal roundtrip time and t_1 is the transmission coefficient of the laser mirror through which light is injected. The frequency ω_R characterizing RO can be expressed as $\omega_R = \sqrt{\xi\Gamma_0|E_0|^2}$ [13].

Equations (2) are written in the frame of the free running laser frequency ω_{sol} and they form a three-dimensional, periodically driven dynamical system. We transform (2) into a convenient form by rescaling the electric field with respect to E_0, and time by ω_R^{-1}. Furthermore, we introduce the new population inversion n and express $\hat{\omega}$ in units of ω_R:

$$\tilde{E} = \hat{E}/E_0, \; n = \xi(N - N_0)/\omega_R, \; \omega = \hat{\omega}/\omega_R,$$

$$t = \hat{t}\omega_R. \qquad (4)$$

Thus Eqs. (2) can be expressed as

$$\dot{\tilde{E}} = \tfrac{1}{2}(1 + i\alpha)n\tilde{E} + Ke^{i\omega t}$$

$$\dot{n} = -2\Gamma n - (1 + 2Bn)(|\tilde{E}|^2 - 1), \qquad (5)$$

where the dot indicates the derivative with respect to the rescaled time t. Furthermore, $B = \omega_R/2\Gamma_0$ is the rescaled cavity lifetime of photons, $\Gamma = \tfrac{1}{2}(\Gamma_N/\omega_R + 2B)$ is the rescaled damping rate of the RO and the dimensionless injected field strength K is $(\kappa E_{inj})/(\omega_R E_0)$.

System (5) is mathematically a three-dimensional vector field, referred to as nonautonomous because its right-hand side depends explicitly on time. This implies that its three-dimensional flow is time-dependent. To get rid of this explicit time dependence we introduce the phase difference $\eta(t) = \omega t - \phi(t)$ between output and input of the laser and substitute $E(t) = \tilde{E}(t)e^{-i\omega t} = r(t)e^{-i\eta(t)}$. Equations (5) can now be rewritten in polar coordinates as

$$\dot{r} = \tfrac{1}{2}nr + K\cos\eta$$

$$\dot{n} = -2\Gamma n - (1 + 2Bn)(r^2 - 1) \qquad (6)$$

$$\dot{\eta} = \omega - \tfrac{1}{2}\alpha n - K\frac{\sin\eta}{r},$$

with the decoupled equation for the phase of the electric field

$$\dot{\phi} = \tfrac{1}{2}\alpha n + K\frac{\sin\eta}{r}.$$

Consequently, one only needs to study the dynamics in (r,n,η)-space of the three-dimensional autonomous vector field Eqs. (6), which is the system studied in Ref. [15]. Alternatively, we can rewrite Eqs. (5) in terms of the complex electric field $E = E_x + iE_y$ as

$$\dot{E} = K + \left(\tfrac{1}{2}(1 + i\alpha)n - i\omega\right)E \qquad (7)$$

$$\dot{n} = -2\Gamma n - (1 + 2Bn)(|E|^2 - 1).$$

We have transformed the three-dimensional nonautonomous vector field (5) into the three-dimensional autonomous (without explicit time dependence) vector fields (6) or (7). Note that mathematically, the time-$2\pi/\omega$ map of the flow of Eqs. (7) is equal to the Poincaré or stroboscopic map for the forcing frequency $2\pi/\omega$ of system Eq. (5); see [15] for

details. Physically, we just changed the frequency of reference from ω_{sol} in Eqs. (5) to ω_{inj} in Eqs. (7).

So far, people have mostly been working with Eqs. (6) (or similar equations) in polar coordinates. The phase space of the system is $R^+ \times R \times (-\pi, \pi]$, which is a half-cylinder. The cylinder is obtained by identifying the line $\{\eta = -\pi\}$ with the line $\{\eta = \pi\}$ in (r,η,n)-space, which is called the covering space. This is possible because Eqs. (6) have the symmetry $\eta \mapsto \eta + 2\pi$. Then only the upper half of the cylinder needs to be considered, because Eqs. (6) also have the symmetry $(r,\eta) \mapsto (-r, \eta + \pi)$. As a consequence, there is a qualitative difference between a limit cycle with bounded or trapped phase difference η, and a limit cycle with unbounded phase difference η (also called a running solution) that runs around the cylinder. As we will see later, a bounded-phase limit cycle can become an unbounded-phase limit cycle, which is a bifurcation of Eqs. (6).

The phase space of Eqs. (7) on the other hand is R^3, and on the level of phase portrait of (7) a limit cycle with bounded phase cannot be distinguished from a limit cycle with unbounded phase. The difference is that a limit cycle with bounded phase difference does not surround the origin in the E-plane, but an unbounded one does. When a bounded-phase limit cycle develops unbounded phase it simply crosses the N-axis in (E,N)-space, which is not a bifurcation. Because of this it is of great advantage to follow limit cycles and their bifurcations, for example period-doublings, in Eqs. (7) where this can be done irrespective of whether the limit cycle has bounded or unbounded phase. This new realization is extremely helpful during computations and we mainly work with Eqs. (7).

There are five parameters appearing in Eqs. (7), of which the injected field strength K and the detuning ω are most important because they can be changed during an experiment. On the other hand, the parameters α, B and Γ are fixed during an experiment as they are given by the material properties of the laser. Of these fixed parameters the linewidth enhancement factor α is the most important in this study. This is why we construct bifurcation diagrams in the two-dimensional (K,ω)-plane for different but fixed α, where we fix B and Γ to the physically realistic values of $B = 0.015$ and $\Gamma = 0.035$ [14]. Notice that there is the further symmetry

$(\omega, \alpha, E) \mapsto (-\omega, -\alpha, E^*)$ of Eq. (7) involving the parameters. This allows us to restrict to positive values of α and get the results for negative α by this symmetry. (Note that semiconductor lasers with negative α may become available in the not too distant future.) Furthermore, this symmetry means that the (K, ω)-plane has the symmetry $\omega \mapsto -\omega$ for $\alpha = 0$, which, to a good approximation, is the case for gas or Nd:Yag lasers [10]. Recall that Eqs. (7) describe a single-mode laser, so that the model is valid as long as the detuning ω does not interfere with the longitudinal mode spacing of the laser.

An experimentally important parameter is the pump current I, and it is incorporated in $K \sim 1/\sqrt{I - I_{thr}}$ through E_0. In fact, one should interpret the injected field strength K as a ratio between the injected field amplitude and the laser field E_0. Hence, increasing K in an experiment is equivalent to either increasing the amount of the injected light or de-

creasing the pump current. Note, however, that we cannot decrease the pump current to reach its threshold value I_{thr} because then the electric field E_0 goes to zero and so K would not be well-defined.

As we already mentioned, the electric fields E and E_0 as well as E_{inj} are written in units of photon numbers. To allow comparisons between our results and experiments, the expressions for the power and unscaled frequency of the electric field injected into the laser are

$$P_{inj} = K^2 \left(\frac{\omega_R}{\kappa} \right)^2 \frac{R_1}{(1 - R_1)^2} P_0, \quad \omega_{inj} = \omega \omega_R + \omega_{sol}.$$

$$(8)$$

Here P_0 is the power that the free-running laser emits from its facet with power reflectivity R_1, through which light is also injected.
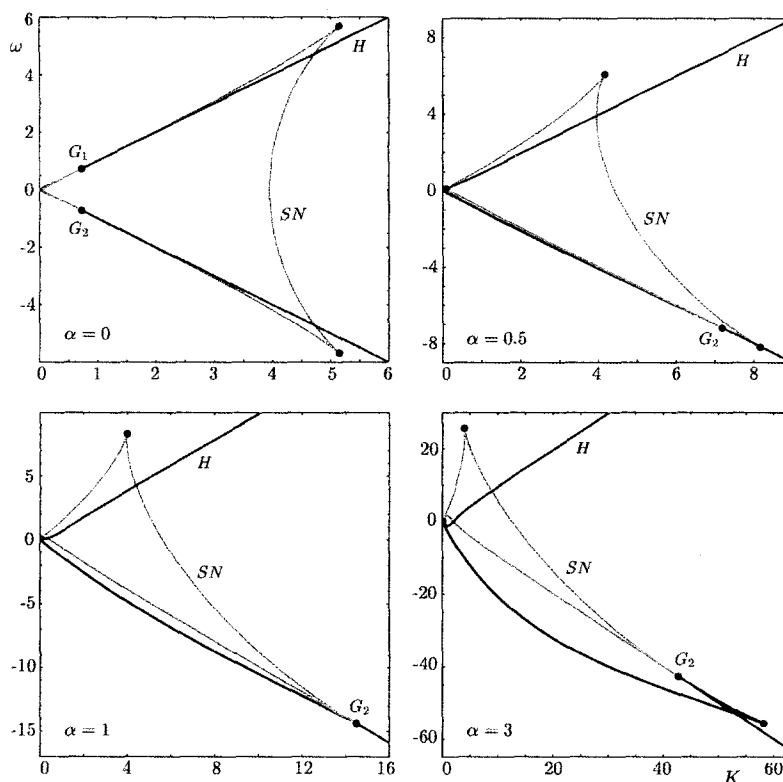

Fig. 1. The bifurcations of stationary points in the (K, ω)-plane are the red Hopf bifurcation curve H and the blue saddle-node bifurcation curve SN. These curves touch at two codimension-two saddle-node-Hopf points G_1 and G_2. Notice also the cusp bifurcation points on SN and the strong dependence of the bifurcation curves on α.
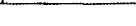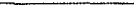
3. The bifurcation diagram

In this section we present our results as bifurcation diagrams in the (K, ω)-plane; as general references to bifurcation theory see for example Ref. [38,39]. As mentioned earlier, we show the dependence of the dynamics on K and ω for a fixed $B = 0.015$ and $\Gamma = 0.035$ and different but fixed values of α.

Each point in the (K, ω)-plane corresponds to a particular phase portrait. Typically, such a phase portrait does not change qualitatively when K and ω are changed a little. However, there are bifurcation points in this plane at which one can observe qualitative changes in phase space. Note that the term *qualitative change* is well defined in bifurcation theory; see Refs. [38,39] for details. The minimum number of parameters necessary to describe such a bifurcation is called its codimension. The basis of the bifurcation diagram is formed by the bifurcations of codimension one, which form curves in the (K, ω)-plane. Where two such curves intersect one finds a bifurcation of codimension at least two. We used the package AUTO [35] to compute codimension-one bifurcation curves of stationary points and limit cycles, which from the backbone of the dynamics of system (7). Note that our approach gives a more global view of the dynamics than the bifurcation diagrams one typically finds, where one phase space quantity is plotted against a single parameter.

Because there is an amazing complexity of bifurcations we introduce them one by one in a convenient order. First we present bifurcations of stationary points, namely saddle-node and Hopf bifurcations. They define the region of locking where the laser produces constant output at the frequency of the injected light. Then we add bifurcations of limit cycles, period-doubling, saddle-node of limit cycle and torus bifurcations, which are particularly important for finding the locations of global bifurcations and chaotic dynamics. We show the bifurcation diagrams in Figs. 1 through 7 in different windows of the (K, ω)-plane, from an overall view to enlargements near the range of small K and ω. To distinguish between bifurcations we use the color coding given in Table 1. Each bifurcation has a different base color, and the darker tone of a color stands for a bifurcation of an attracting object, called a supercriti-

Table 1
The color coding of the curves of different bifurcations

Type of bifurcation	Symbol	Color coding	
		supercritical	subcritical
Saddle-node	SN	▮▮▮	▨▨▨
Hopf	H	▮▮▮	▨▨▨
Period-doubling	P	▮▮▮	▨▨▨
Saddle-node of limit cycle	SL	▮▮▮	
Torus bifurcation	T	▮▮▮	▨▨▨

cal bifurcation. The lighter tone of a color represents a subcritical bifurcations in which no attractors are born. In simulations or experiments only attractors are found, so that the darker colored curves are more relevant from a practical point of view. However, we stress that it is a strength of our method that we can compute also the curves of subcritical bifurcations which are necessary to obtain an overall and consistent picture. What is more, subcritical bifurcation curves may change their stability and become supercritical, for example when α changes. To further distinguish between bifurcation curves of periodic orbits of basic period and those that have already undergone a period-doubling, the latter are represented by thinner curves. We also indicate this in superscript in the labeling.

For the physical interpretation of different phase portraits of Eqs. (7) recall that the system is written in the reference frame of the injection frequency ω_{inj}. The time derivative of the phase η of E corresponds to the difference between the laser instantaneous resonant frequency and the injected signal frequency. A stationary point then corresponds to an output with constant intensity, population inversion and phase, which means that the frequency is that of the injected field. A limit cycle with bounded phase η describes an exchange of energy between electric field and population inversion, relaxation oscillations being the typical example. A limit cycle with unbounded phase (running phase) corresponds to an output with oscillating intensity and a frequency that is the free running laser frequency shifted according to the new average carrier density caused by injection. Superposition of the laser field and the injected field which have different frequencies results in beating, that is, the signal oscillates with the optical

frequency but is modulated on a scale determined by the detuning between the component fields. In this case, oscillations in the intensity of an unbounded limit cycle correspond to the offset of the beating between the laser frequency and the frequency of the injected light. An invariant torus in the system corresponds to a competition between two oscillators and is characterized by the frequencies of these oscillations in the spectrum. On an invariant torus trajectories can either converge to an attracting periodic orbit or densely fill the torus, in which case the dynamics is quasiperiodic. The boundaries between these two different kinds of dynamics are formed by curves of saddle-node of limit cycle bifurcations, which form the well known resonance or Arnol'd tongues.

4. Bifurcations of stationary points

In this section we describe local bifurcations of stationary points, saddle-node and Hopf bifurcations, and also discuss more global aspect of their organization. There exist two codimension-two bifurcation points of a simultaneous saddle-node and Hopf bifurcation where there is a tangency between the corresponding bifurcation curves.

4.1. Saddle-node and Hopf bifurcation

In Fig. 1 are shown in blue the curve SN of saddle-node bifurcations and in red the curve H of Hopf bifurcations in four panels for different representative values of α. In the saddle-node bifurcation two stationary points are created that exist in the
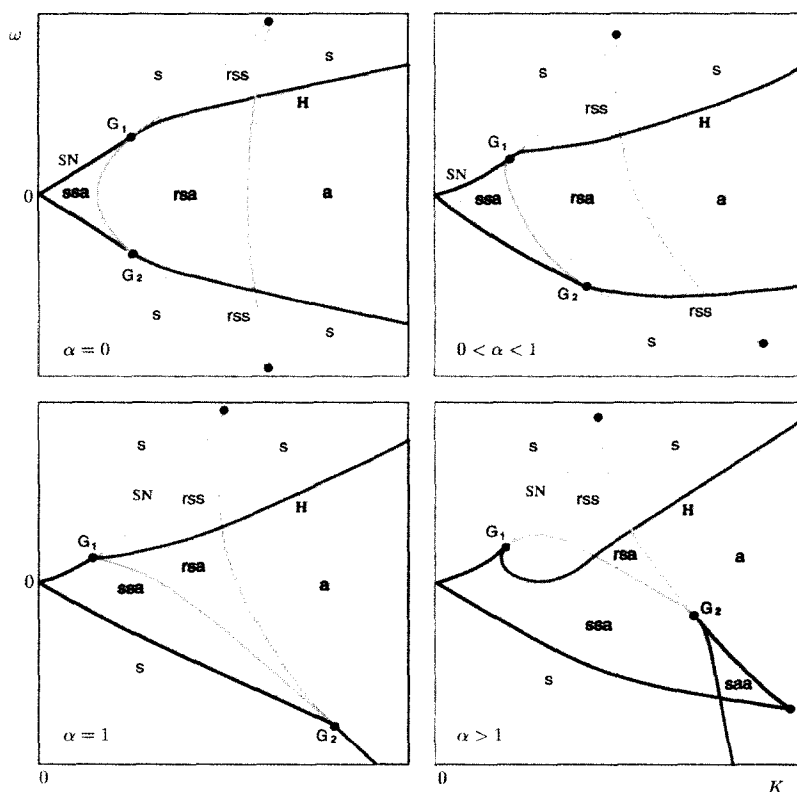

Fig. 2. Qualitative sketches of the bifurcation curves in Fig. 1 with symbols indicating the stability of stationary points, where a stands for an attractor, r for a repellor, and s for a saddle point. The shaded region is the locking range.

triangle-shaped region bounded by *SN*. One of the bifurcating stationary points is an attractor where the curve *SN* is dark blue, but along the light blue curve a repellor and a saddle point bifurcate. The two far corners of the curves *SN* are formed by codimension-two cusp bifurcations, where three stationary points bifurcate. The adjoining branches of *SN* correspond to saddle-node bifurcations of different pairs of stationary points. Along the curve *H* a stationary point bifurcates with a limit cycle. The dark red part of *H* corresponds to a supercritical Hopf bifurcation creating an attracting limit cycle, whereas the light red part corresponds to a subcritical Hopf bifurcation with the emergence of an unstable limit cycle. The changes from super- to subcritical along both *SN* and *H* occur where the two curves become tangent at the codimension-two points G_1 and G_2.

The curves *SN* and *H* divide the (K, ω)-plane into regions of different numbers and stability of stationary points. To highlight this we sketch in Fig. 2 the different qualitative cases for different values of α. A region of the (K, ω)- plane is labeled with the symbols *a*, *r* and *s* depending on whether there is a stationary point that is attracting, repelling or a of saddle-type. Whenever there is an attractor the laser locks to the input, which defines the shaded locking region in Fig. 2.

It turns out that the two stationary points born along the dark blue part of *SN* are created in a saddle-node bifurcation on a limit cycle (or saddle-node infinite-period bifurcation [32]). The limit cycle exists outside *SN* and its period goes to infinity. Then a saddle-node appears on the limit cycle, which develops into two stationary points on an invariant circle; the situation is sketched in Fig. 3. The saddle-node bifurcation does not occur on a limit cycle along the entire curve *SN*: this happens near the point G_1 and before a codimension-two homo-

clinic saddle-node bifurcation is reached; compare [33].

As was mentioned earlier, there are two saddle-node-Hopf bifurcation points G_1 and G_2 where *SN* and *H* are tangent. These codimension-two bifurcation points are known to generate very complicated dynamics in their vicinity. The dynamics near G_1, which is in the region of small *K* and ω, was studied in [12,14,15,33]. This revealed the existence of torus bifurcations (also discussed below) as well as homoclinic and heteroclinic bifurcations. On the other hand, there is not much known about G_2. This point was mentioned in Ref. [27] but has not been studied so far. Preliminary work shows that the local structure near G_2 is similar to that of G_1, but with the extra difficulty of slow-fast dynamics. How this organizes the dynamics near G_2 is beyond the scope of this paper and will be discussed elsewhere.

Figs. 1 and 2 show that there is a strong qualitative dependence of the bifurcation diagram on α. For $\alpha = 0$ the bifurcation diagram is symmetric. The panel for $\alpha = 0.5$ of Fig. 1 is representative for the qualitative situation for $0 < \alpha < 1$, where the point G_2 shifts towards bigger *K*-values as α approaches 1, but remains on the lower branch of *S*. A very special situation occurs for $\alpha = 1$ because *H* has a cusp at G_1 and also goes through the cusp on *SN* at the point G_2, which makes this a bifurcation of codimension at least three. The panel for $\alpha = 3$ of Fig. 1 represents the qualitative situation for any $\alpha > 1$. Increasing α above 1 results in *H* developing a fish-like shape near G_1, resulting in a characteristic shape of the locking range; compare Fig. 2. Increasing the injection strength *K* for small positive detuning ω results in locking at first, then unlocking and then again locking as *K* grows; compare for example [28]. For $\alpha > 1$ there also exists a region with two attracting stationary points near G_2. This bistability is already pointed out in [27]. Bistable behavior in a resonant optical amplifier, which in fact is very similar to an optically injected laser, was studied in [40]. Because the bistability occurs for large injected power and large negative detuning, we conclude that this is a manifestation of dispersive optical bistability [41]. This is known to occur in Fabry-Perot interferometers with power-dependent refractive index and must therefore also be expected in a laser with non-zero α [42].
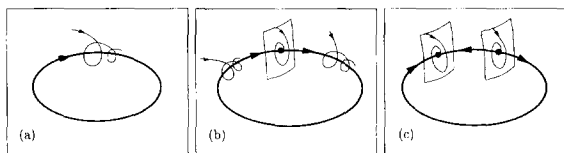

Fig. 3. Sketch of phase portraits before (a), exactly at (b) and after (c) the saddle-node bifurcation on a limit cycle that occurs when the dark blue part of the curve *SN* is crossed in Figs. 1 and 2.

Finally, α affects the bifurcation diagram not only qualitatively, but also quantitatively. There is quite a change in the range of the relevant values of K and ω with increasing α, as can be read off from the scaling of the panels in Fig. 1.

All figures in this paper show that the locking region becomes asymmetric with respect to positive and negative detuning ω when the parameter α increases: for $\alpha > 0$ one has to inject more light in order to obtain locking for positive ω than for negative ω. Also the opening angle between the two branches of the curve SN (see Fig. 1) emerging from $(K,\omega) = (0,0)$ increases with α. To understand this recall the property of the linewidth enhancement factor α that

$$\alpha \propto -\frac{\partial n_r / \partial N}{\partial g / \partial N}. \qquad (9)$$

Here n_r is the refractive index, g is the optical gain and N is the population inversion. The instantaneous resonance frequency of the laser is inversely proportional to the refractive index n_r. Nonzero α therefore means that the instantaneous resonance frequency of the laser shifts if the inversion N changes (at fixed pump current). Moreover, injection usually causes a decrease of the population inversion which, for positive α, results through the increase of the refractive index in a downshift of the instantaneous resonance frequency. At the same time the output power increases. Because of this frequency downshift the laser can achieve locking for negative detuning ω at a much smaller injection level than for positive ω. For $\alpha = 0$ this asymmetry is not present. The increasing opening angle of SN occurs because bigger α means more significant changes in the laser instantaneous resonance frequency for the same amount of injected light; see Eq. (9). Thus, as α increases less and less light has to be injected to obtain locking for a given negative detuning ω.

5. Dynamics of limit cycles

Along the Hopf bifurcation curve H discussed in the last section a limit cycle is created, and we now study what may happen to this and other limit cycles. To this end we consider the Floquet multipliers, which are the eigenvalues of the Poincaré return map

on a suitable section transverse to the limit cycle. A limit cycle changes stability when Floquet multipliers cross the unit circle in the complex plane, and there are three different codimension-one bifurcations: period-doubling when a Floquet multiplier goes through -1, saddle-node of limit cycles when a Floquet multiplier goes through 1, and torus bifurcation (Neimark-Sacker bifurcation of the Poincaré map) when a pair of complex conjugate Floquet multipliers crosses the unit circle. With the package AUTO [35] these bifurcations can be detected and followed in parameter space. This allows us to map out the dynamics and bifurcations of limit cycles in great detail. We also look at the phase unbounding of limit cycles and other objects, which has physical meaning although it is not a bifurcation of system (7).

5.1. Period-doubling bifurcation

The curves of period-doubling bifurcations are shown in green in Fig. 4, added to the curves SN and H of stationary points. They are denoted by P^1 when a limit cycle of basic period undergoes a bifurcation, and P^2 when the bifurcating limit cycle has twice the basic period, in which case the curve is also plotted thinner. Dark green corresponds to supercritical period-doubling of an attracting limit cycle, and light green to subcritical period-doubling of a non-attracting limit cycle. Note that the curves form closed loops.

The attracting limit cycle born on the dark red branch of the Hopf curve H undergoes successive period-doublings when the dark green P^1 and P^2 are crossed. On the other hand, the repelling limit cycle born on the light red branch of H period-doubles on the light green part of P^1. The color of a period-doubling curve may change from light to dark green, which indicates a change from sub- to super-critical. This codimension-two bifurcation is the consequence of an intersection with a torus or saddle-node of limit cycle curve, as will be discussed below. The curves P^1 and P^2 in Fig. 4 are the first two steps in a period-doubling cascade to chaos. Higher period-doubling curves are not shown here in order to keep the figure simple, but they lie inside each other and accumulate according to
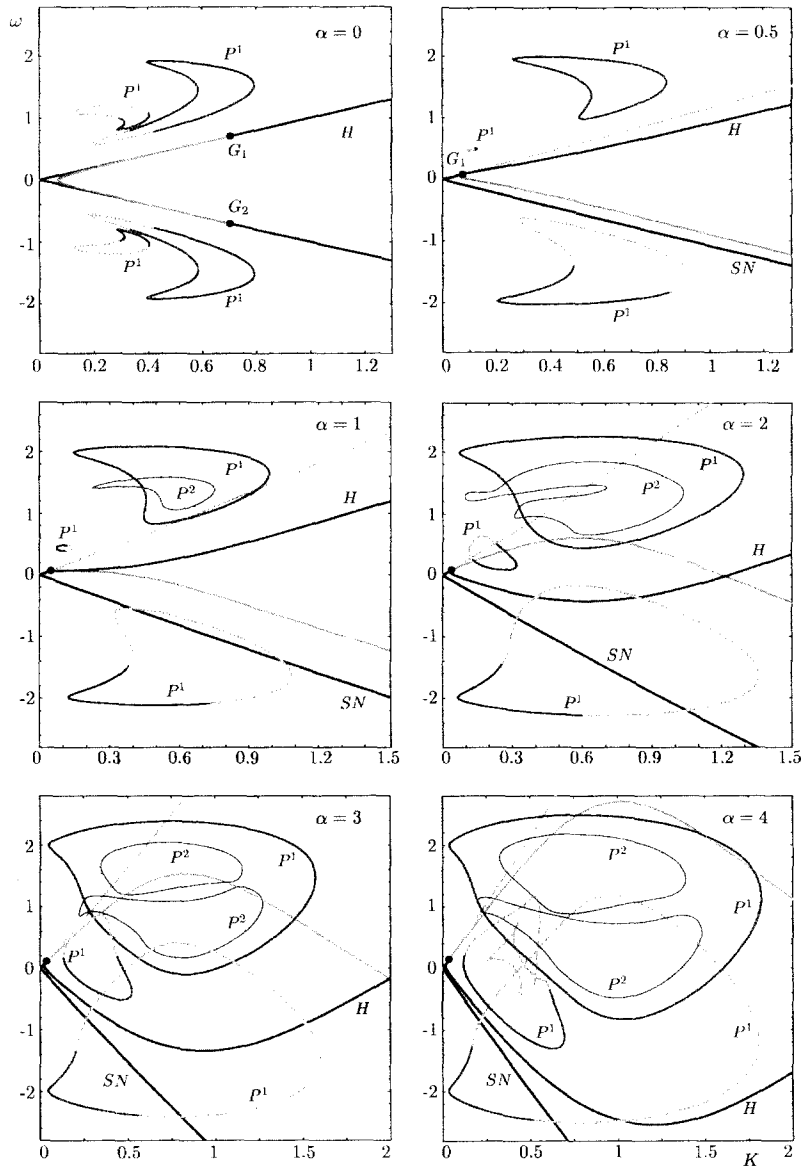
Fig. 4. Curves of period-doubling bifurcations in green, which turn out to form closed loops. Notice how the overall structure of period-doublings becomes more complex as α increases. The superscripts indicate multiples of the basic period; see Table 1 for the color coding.

Feigenbaum's universal scaling law. The resulting chaotic islands will be studied in detail elsewhere, but the curves P_2 in Fig. 4 already give a good indication where chaos is located.

The period-doubling route to chaos was the subject of a number of theoretical and experimental papers. It was usually presented in two ways: in the form of isolated pieces of bifurcation curves in the (K, ω)-plane [11,13,22,29] and by plotting maxima and minima of an amplitude of periodic orbits as a function of one parameter [17–21]. All earlier results fit nicely into the overall picture presented here. An

inverse period-doubling cascade back to the period one limit cycle was also observed [18,20]. This can now be explained by the shape of the period-doubling curves in Fig. 4. Most striking is the similarity between the experimental stability map of an injected semiconductor laser reproduced in Fig. 8 from [22] and our theoretical results in the panels $\alpha = 3$ and $\alpha = 4$ in Fig. 4.

The period-doubling curves show a remarkable sensitivity to a variation of α. They grow in the (K, ω)-plane as α increases and become more complicated in shape by developing self-intersections. Furthermore, the curve P_2 splits up into two isolas for α between 2 and 3. Period-doubling to chaos for zero detuning when K is increased has been found in semiconductor lasers [18,31]. However, we con-
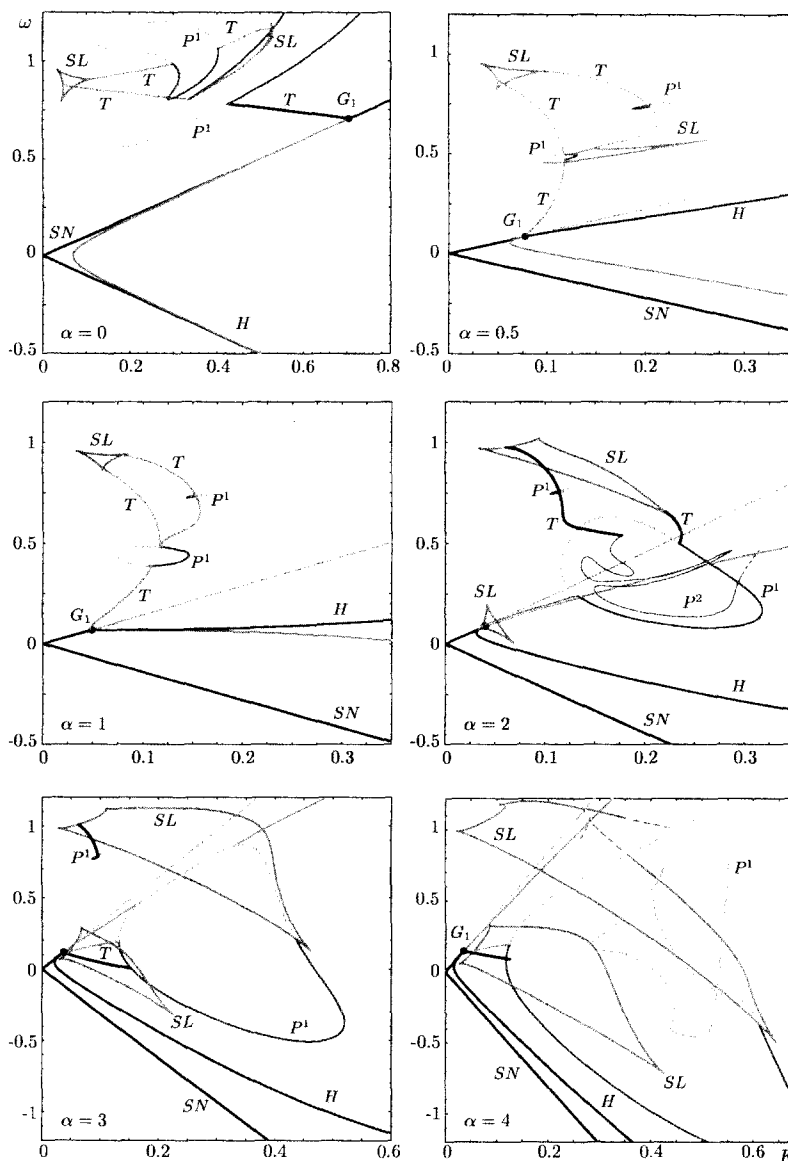

Fig. 5. A series of bifurcation diagrams showing the intricate connection between period-doubling, saddle-node of limit cycle and torus bifurcations. The superscripts indicate multiples of the basic period; see Table 1 for the color coding.
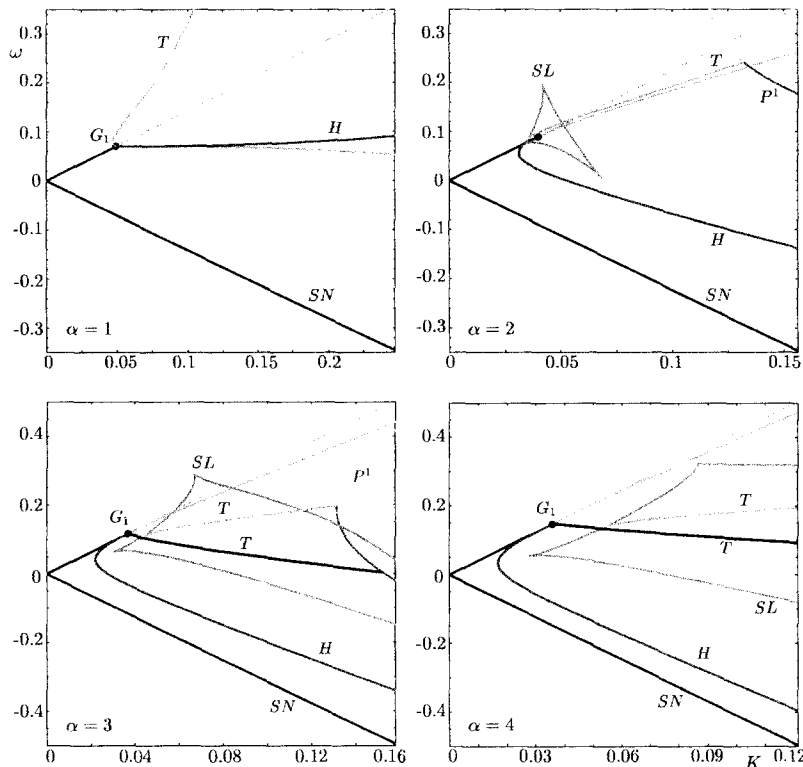
Fig. 6. A series of bifurcation diagrams in a neighborhood of the saddle-node-Hopf point G_1; compare [14,15]. Notice the torus curves emerging from G_1 and the changes with increasing α. See Table 1 for the color coding.

clude that this can only be the case for larger values of α, because the period-doubling curves do not cross the axis $\omega = 0$ for $\alpha < 3$. We expect that it is possible to confirm this prediction experimentally in VCSELs.

5.2. Saddle-node of limit cycle bifurcation

The saddle-node of limit cycle bifurcation curves, denoted SL, are shown in Figs. 5–7 in brown. In Fig. 7 there is a saddle-node of limit cycle curve SL^2 of a limit cycle of twice the basic period, which is also drawn as a thinner curve. This bifurcation results in the creation of two limit cycles, namely of a saddle limit cycle with either an attracting limit cycle in the supercritical case or a repelling limit cycle in the subcritical case. The supercritical case is one of the mechanisms leading to bi- or multistability. The curves SL generally form closed loops with a number of cusps in them, and they bound a region in the

(K, ω)-plane where there is an attracting or repelling limit cycle. The meaning of the cusp is the same as for fixed points: two different pairs of limit cycles bifurcate when SL is crossed on different sides of a cusp. The regions bounded by saddle-node of limit cycle curves can be, but do not have to be, resonance tongues of a torus. In the figures there are several curves of torus bifurcations, which will be discussed in the next section, and attached to each of them there are infinitely many resonance tongues. Here we only show the most prominent saddle-node of limit cycle curves, which are responsible for bi- or even multistability.

The curves SL change significantly with a variation of α. They grow in parameter space as α increases and become very complicated in shape by developing extra cusps (in codimension-three swallow tail bifurcations). In order not to overcrowd Fig. 5 we plot only the most significant parts of curves; dashing indicates that a curve continues.
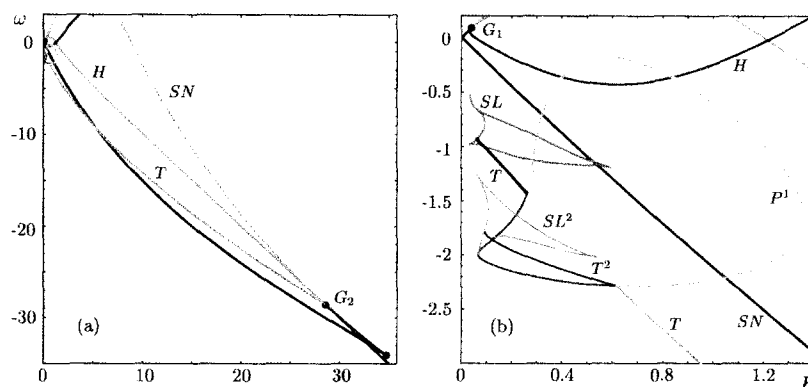
Fig. 7. The torus curve T emerging from the saddle-node-Hopf point G_2 (a) extends all the way to a region of small values of K and negative ω (b), where it is involved in a complex structure with other bifurcations of limit cycles. The superscripts indicate multiples of the basic period; see Table 1 for the color coding. The panels are for $\alpha = 2$

5.3. Torus bifurcation

The existence of quasiperiodicity and the existence of tori in laser systems was reported in [10,23] for injected gas lasers ($\alpha = 0$) and then also for semiconductor lasers in [11,12,15,28,29,31]. Here we present these torus bifurcation curves that are responsible for color changes of period-doubling curves and those which start in the vicinity of the points G_1 and G_2. The torus bifurcation curves, denoted by T, are shown in Figs. 5–7 in black or gray. Along a black supercritical curve T an attracting torus is born from an attracting limit cycle, whereas repelling tori are born along gray subcritical curves T. In Fig. 7 there is a thin torus bifurcation curve T^2 of a limit cycle of twice the basic frequency. The dynamics on the bifurcating torus is either quasiperiodic or there is an attracting limit cycle on the torus with a rational rotation number. The regions in which such limit cycles exist are the resonance tongues, and their boundaries are formed by saddle-node of limit cycle curves. We did not draw these resonance tongues in the figures in order to keep them as clear as possible.

There are several types of torus curves in the figures. In Figs. 5 and 6 one can see torus curves associated with the codimension-two saddle-node-Hopf point G_1. In [29] an approximation was presented that predicts a torus curve connecting G_1 in an arc with the point $(K, \omega) = (0, 1)$. Here we present in panels $\alpha = 0.5$ through $\alpha = 3$ of Fig. 5 the upper part of this curve. It starts at SL and is divided by a small period-doubling loop at $\omega \approx 0.75$ before it

ends at a larger period-doubling loop. Its bottom part (the curve l in [15]) is not presented here but there is a second, subcritical T curve emerging from G_1 which is shown in panels $\alpha = 0.5$ through $\alpha = 4$ of Fig. 5. For low values of α it is not always below SN, and it turns out to interfere with a saddle-node of limit cycle curve SL lying very close to G_1. An extra attracting torus curve appears close to the unstable torus curve for larger values of α; see Figs. 5 and 6. (This curve is recognized as the curve H discussed in detail in [15].) The existence of quasiperiodic oscillations of different stability in the vicinity of G_1 was also reported by Lee et al. [11]. The second type of torus curve is associated with the codimension-two point G_2 as shown in Fig. 7(a). A curve T starts at G_2 and extends all the way to small values of K and ω; an approximate formula for this curve can again be found in [29]. However, the organization of bifurcations is quite intricate and torus curves are responsible for stability changes of period-doubling curves for negative detunings. They are the third type of torus curves we find, connecting saddle-node of limit cycle curves with period-doubling curves. These curves are responsible for changes of stability along period-doubling curves and generally provide a connection between bifurcations that seem to be independent of each other at first glance.

5.4. The overall picture of bifurcations

We presented one by one several kinds of bifurcations which form the backbone of the dynamics of an

injected (semiconductor) laser. Many of these bifurcations were studied before, but they were often treated as unconnected and isolated from each other. However, this is not the case at all because the different bifurcations form a complicated structure of interrelated and interlinked objects as is evidenced by Figs. 5 and 6. The key to understanding the system is looking at the relationships between different phenomena which turn out to influence each other. For example, period-doublings have been studied separately, and in Fig. 4 one may indeed get the impression that the period-doubling bifurcation curves are isolated from the rest of the bifurcations. However, they do change from super- to subcritical (1:2 resonance) and, following the nature of the problem, one finds torus bifurcations interacting with the period-doublings causing this change as pictured in Fig. 5. The torus bifurcation curves in turn connect to saddle-node of limit cycle bifurcation curves (1:1 resonance) and some of them have their origin at the points G_1 and G_2. In this way all bifurcations interact and organize the overall dynamics of the system.

The overall picture of bifurcation curves in the (K, ω)-plane is in very good agreement with the experimental stability map reproduced from [22] in Fig. 8. If one compares the experimental bifurcation diagram with panels $\alpha = 3$ and $\alpha = 4$ of Fig. 4 one notices great similarity, where the supercritical branch of the Hopf bifurcation provides a good reference. The boundaries between the regions P1 and P2 with a limit cycle of basic period and twice
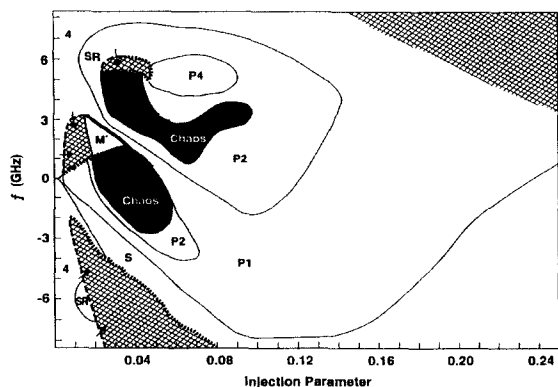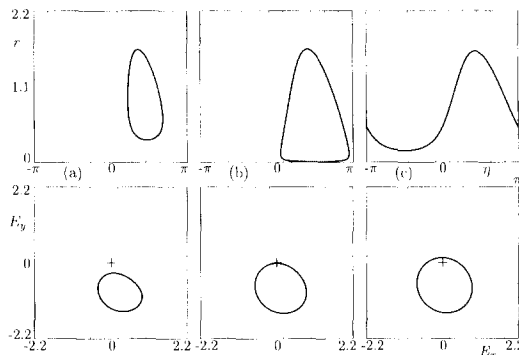

Fig. 9. Phase unbounding of an attracting limit cycle for $\alpha = 3$ and $K = 1.7$ shown in the (η, r)-plane of Eqs. (6) (top row) and projected onto the complex E-plane of Eqs. (7) (bottom row) for $\omega = 0.6$ (a), $\omega = 1.56$ (b), and $\omega = 2.2$ (c).

the basic period in Fig. 8 agree well with the curves P^1 in Fig. 4. Our results shed light on the nature of the regions denoted by 'chaos' in Fig. 8. These regions coincide with the area confined by the secondary period-doubling curves P^2. Moreover, we expect chaotic dynamics due to the break-up of tori in the regions of so-called subharmonic resonance SR in [22]. In short, the overall picture of interconnected bifurcation curves presented here truly forms the backbone of the dynamics that have been found experimentally.

5.5. Phase unbounding

The limit cycle that exists for very low injection corresponds to a physical process that can be approximated by four-wave mixing due to a nonlinear interaction between the external field, the laser field and the inversion inside the laser [16,43]. By increasing the injection strength the region of multi-wave mixing is entered up to the moment when the phase of the limit cycle becomes bounded. This means that the injection is strong enough to force the laser to lase at the same average frequency as the input. In the polar coordinate description of Eqs. (6) this is a bifurcation. However, in Eqs. (7) this merely means that an attracting limit cycle has crossed the n-axis, so that in projection onto the E-plane it now surrounds the origin.

This is why we can numerically follow a limit cycle of Eqs. (7) irrespective of whether its phase is bounded or unbounded. This important fact is the
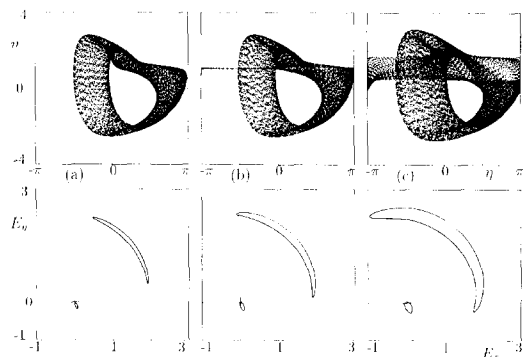

Fig. 8. Experimental stability map of an injected semiconductor laser by Simpson et al. reproduced from [22].

Fig. 10. Phase unbounding of a repelling torus for $\alpha = 1$ and $\omega = 0.38$ shown in the (η, r)-plane of Eqs. (6) (top row) and projected onto the complex E-plane of Eqs. (7) (bottom row) for $K = 0.1575$ (a), $K = 0.1585$ (b), and $K = 0.163$ (c).

Fig. 12. Period doubling route to chaos for $\alpha = 2$ and $K = 0.625$ shown as attractors in the E-plane of the Poincaré map defined by the section $\{n = 0\}$. From (a) to (f) ω takes the values 0.3, 0.5, 0.7, 0.71, 0.78, and 1.1.

main reason why we chose to work with Eqs. (7) rather than with Eqs. (6). In Fig. 9 the transition from a bounded-phase limit cycle to a unbounded-phase limit cycle is shown for Eqs. (6) and Eqs. (7), respectively. It is clear from Fig. 9 (top row) that the bounded phase limit cycle cannot be continued in Eqs. (6), but there is no problem when one works with Eqs. (7) (bottom row). The unbounding of the phase can also occur for a torus or even a chaotic attractor, as is shown in Figs. 10 and 11. Notice how the torus and the attractor start to become unbounded in quite a spectacular fashion in the top row, whereas there is no qualitative change in the bottom row.

Phase-unbounding is important from the physical point of view because it constitutes the upper bound-
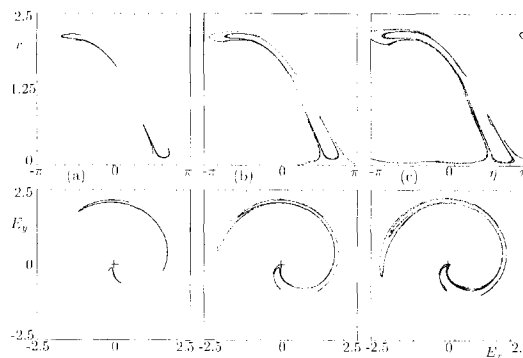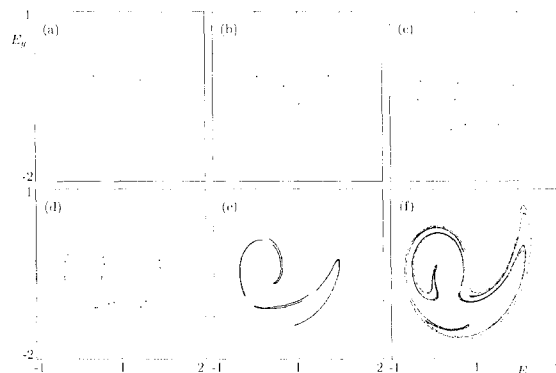
ary of the bounded phase dynamics. This can be detected in experiments because the laser stops to operate at an average frequency, which is that of the injected light. Notice however that there are regions of multistability in the (K, ω)-plane in which there are coexisting attracting objects (limit cycles, tori, chaotic attractors). For each such attractor the phase becomes unbounded for slightly different parameter values, so that there is not a single well-defined curve of phase-unbounding. On the other hand, when there is a single attractor this curve is well defined.

6. Routes to chaos

As we already mentioned in Section 1 many different routes to chaos have been reported for (semiconductor) lasers with optical injection. Transitions to chaotic behavior via period-doubling cascades, intermittencies and another instabilities were observed experimentally [7,17–21,31] as well as in a various numerical simulations based on the rate equations [10,11,16–21,31].

For illustration we picture two transitions to chaos, which are closely associated with the bifurcation curves we computed in the (K, ω)-plane. Fig. 12 shows with a series of attractors of the Poincaré map (computed with DsTool [44]) in the section $\{n = 0\}$ how an attracting limit cycle period-doubles repeatedly and becomes a chaotic attractor. The parameters are chosen so that the isolas of nested period-dou-
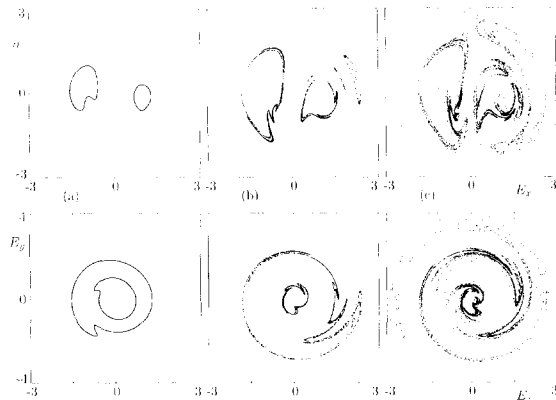

Fig. 11. Phase unbounding of a chaotic attractor for $\alpha = 2$ and $K = 0.241$ shown in the (η, r)-plane of Eqs. (6) (top row) and projected onto the complex E-plane of Eqs. (7) (bottom row) for $\omega = 0.16$ (a), $\omega = 0.17$ (b), and $\omega = 0.2$ (c).

Fig. 13. Break-up of an attracting torus for $\alpha = 2$ shown simultaneously in the (E_x, n)-plane of the Poincaré map defined by the section $\{E_y = 0\}$ (top row) and in the E-plane of the Poincaré map defined by the section $\{n = 0\}$ (bottom row). The parameter values are $\omega = 0.7$, $K = 0.124$ (a), $\omega = 0.7$, $K = 0.152$ (b), and $\omega = 0.6$, $K = 0.179$ (c).

bling bifurcation curves in Fig. 4 are crossed. Fig. 13 shows the break-up of an attracting torus that is born on one of the two T curves from the panel $\alpha = 2$ in Fig. 5. Both top row and bottom row show the same transition, but in the two perpendicular Poincaré sections $\{E_y = 0\}$ and $\{n = 0\}$, respectively. The smooth torus becomes non-smooth and very fractal-like and then develops into full-blown chaos that does not resemble the original torus any longer. Such a torus break-up is due to changing the parameters into a region of overlapping resonance tongues.

7. Conclusion

With advanced tools from bifurcation theory we investigated the organization of the dynamics in the full three-dimensional rate equation model describing a (semiconductor) laser with optical injection. Contrary to earlier works, our results are exact in the context of single-mode rate equations because no further approximations have been made. We presented here a unified picture including different kinds of injected laser behavior and provided an understanding of their interrelationships. Our work incorporates and puts together into one global picture earlier theoretical studies and is in a good agreement with experiments. Combining the entire picture in

the (K, ω)-plane together with its dependence on material properties of the laser, notably the α parameter, gives new insight into the overall dynamics of optically injected semiconductor lasers. This shows that there are qualitative differences in the optically injected laser behavior for different α-values. Starting from a symmetric bifurcation diagram for $\alpha = 0$, the symmetry is gradually lost and the bifurcation curves evolve, grow and become more complex as α increases.

As we already mentioned we are aware that there exist extra bifurcations, like other torus bifurcations [29], homoclinic [12,33] and heteroclinic [12,15] bifurcations, as well as chaotic dynamics connected to them. This is beyond the scope of this paper, which is also intended as a reference for future, more detailed research into the complex dynamics of optically injected lasers.

Acknowledgements

References

[1] R. Lang, IEEE J. Quantum Electron. 18 (1982) 976.
[2] S. Kobayashi, T. Kimura, IEEE J. Quantum Electron. 16 (1980) 915.
[3] F. Mogensen, H. Olesen, G. Jacobsen, Electron. Lett. 21 (1985) 696.
[4] C.R. Mirasso, P. Colet, P. Garcia-Fernández, IEEE Photon. Technol. Lett. 8 (1996) 299.
[5] S. Sinha, W.L. Ditto, Phys. Rev. Lett. 81 (1998) 2156.
[6] G.H.M. van Tartwijk, D. Lenstra, Quant. Semiclass. Opt. 7 (1995) 87.
[7] L.A. Lugiato, L.M. Narducci, D.K. Bandy, C.A. Pennise, Opt. Commun. 46 (1983) 64.
[8] E. Brun, B. Derighetti, D. Meier, R. Holzner, M. Ravani, J. Opt. Soc. Am. B 2 (1985) 156.
[9] J.L. Boulnois, A. van Lerberghe, P. Cottin, F.T. Arecchi, G.P. Puccioni, Opt. Commun. 58 (1986) 124.
[10] J.R. Tredicce, F.T. Arecchi, G.L. Lippi, G.P. Puccioni, J. Opt. Soc. Am. B 2 (1985) 173.

[11] E.-K. Lee, H.-S. Pang, J.-D. Park, H. Lee, Phys. Rev. A 47 (1993) 736.

[12] H.G. Solari, G.L. Oppo, Opt. Commun. 111 (1994) 173.

[13] P.C. de Jagher, W.A. van der Graaf, D. Lenstra, Quant. Semiclass. Opt. 8 (1996) 805.

[14] B. Krauskopf, W.A. van der Graaf, D. Lenstra, Quant. Semiclass. Opt. 9 (1997) 797.

[15] B. Krauskopf, N. Tollenaar, D. Lenstra, Opt. Commun. 156 (1998) 158.

[16] D. Lenstra, G.H.M. van Tartwijk, W.A. van der Graaf, P.C. De Jagher, Proc. SPIE 2039 (1993) 11.

[17] T.B. Simpson, J.M. Liu, A. Gavrielides, V. Kovanis, P.M. Alsing, Appl. Phys. Lett. 64 (1994) 3539.

[18] T.B. Simpson, J.M. Liu, A. Gavrielides, V. Kovanis, P.M. Alsing, Phys. Rev. A 51 (1995) 4181.

[19] T. Erneux, V. Kovanis, A. Gavrielides, P.M. Alsing, Phys. Rev. A 53 (1996) 4372.

[20] V. Annovazzi-Lodi, S. Donati, M. Manna, IEEE J. Quantum Electron. 30 (1994) 1537.

[21] V. Kovanis, A. Gavrielides, T.B. Simpson, J.M. Liu, Appl. Phys. Lett. 67 (1995) 2780.

[22] T.B. Simpson, J.M. Liu, K.F. Huang, K. Tai, Quant. Semiclass. Opt. 9 (1997) 765.

[23] A. Politi, G.L. Oppo, Phys. Rev. A 33 (1986) 4055.

[24] G.L. Oppo, A. Politi, G.L. Lippi, F.T. Arecchi, Phys. Rev. A 34 (1986) 4000.

[25] A. Gavrielides, V. Kovanis, P.M. Varangis, T. Erneux, G. Lythe, Quant. Semiclass. Opt. 9 (1997) 785.

[26] P.A. Braza, T. Erneux, Phys. Rev. A 41 (1990) 6470.

[27] T. Erneux, A. Gavrielides, V. Kovanis, Quant. Semiclass. Opt. 9 (5) (1997) 811.

[28] V. Kovanis, T. Erneux, A. Gavrielides, Opt. Commun. 159 (1999) 177.

[29] M. Nizette, T. Erneux, A. Gavrielides, V. Kovanis, Proc. SPIE 3625 (1999) 673.

[30] F. Mogensen, G. Jacobsen, H. Olesen, Opt. Quantum Electron. 16 (1984) 183.

[31] J. Sacher, D. Baums, P. Panknin, W. Elsäßer, E.O. Göbel, Phys. Rev. A 45 (1992) 1893.

[32] M.K.S. Yeung, S.H. Strogatz, Phys. Rev. E 58 (4) (1998) 4421.

[33] M.G. Zimmermann, M.A. Natiello, H. Solari, Physica D 109 (1997) 293.

[34] B. Krauskopf, N. Tollenaar, W.A. van der Graaf, D. Lenstra, Proc. SPIE 3283 (1998) 589.

[35] E. Doedel, T. Fairgrieve, B. Sandstede, A. Champneys, Yu. Kuznetsov, X. Wang, AUTO 97: Continuation and bifurcation software for ordinary differential equations, http://indy.cs.concordia.ca/auto/main.html.

[36] D. Bossert, D. Gallant, IEEE Photon. Technol Lett. 8 (1996) 322.

[37] J. Hader, D. Bossert, J. Stohs, W.W. Chow, S.W. Koch, J. Moloney, Appl. Phys. Lett. 74 (1999) 2277.

[38] J. Guckenheimer, P. Holmes, Nonlinear Oscillations, Dynamical Systems and Bifurcations of Vector Fields, Second Printing, Springer, 1986.

[39] Yu. A. Kuznetsov, Elements of Applied Bifurcation Theory, Applied Mathematical Sciences 112, Springer, 1995.

[40] G.H.M. van Tartwijk, H. de Waardt, B.H. Verbeek, D. Lenstra, IEEE J. Quantum Electron. 30 (1994) 1537.

[41] L.A. Lugiato, Theory of optical bistability, E. Wolf (Ed.), Progress in Optics, vol. 21, No. 71, North-Holland, Amsterdam, 1984.

[42] W.A. van der Graaf, Optical Bistability in a semiconductor laser, Quantum Electronica Dossier, vol. 93-1, Free University, Amsterdam, The Netherlands, 1993.

[43] G.H.M. van Tartwijk, G. Muijres, D. Lenstra, M.P. van Exter, J.P. Woerdman, Electronics Lett. 29 (1993) 137.

[44] A. Back, J. Guckenheimer, M.R. Myers, F.J. Wicklin, P.A. Worfolk, Notices Amer. Math. Soc. 39 (1992) 303.